



HAL
open science

Cable force estimation method based on UAVs and EMD

Wenjun Luo, Shufan Cai, Limei Zeng, Gongfa Chen, David Bassir

► **To cite this version:**

Wenjun Luo, Shufan Cai, Limei Zeng, Gongfa Chen, David Bassir. Cable force estimation method based on UAVs and EMD. *International Journal for Simulation and Multidisciplinary Design Optimization*, 2024, 15, pp.14. 10.1051/smdo/2024012 . hal-04690925

HAL Id: hal-04690925

<https://hal.science/hal-04690925>

Submitted on 13 Sep 2024

HAL is a multi-disciplinary open access archive for the deposit and dissemination of scientific research documents, whether they are published or not. The documents may come from teaching and research institutions in France or abroad, or from public or private research centers.

L'archive ouverte pluridisciplinaire **HAL**, est destinée au dépôt et à la diffusion de documents scientifiques de niveau recherche, publiés ou non, émanant des établissements d'enseignement et de recherche français ou étrangers, des laboratoires publics ou privés.



Distributed under a Creative Commons Attribution 4.0 International License

Cable force estimation method based on UAVs and EMD

Wenjun Luo¹, Shufan Cai¹, Limei Zeng¹, Gongfa Chen^{1,*}, and David Bassir^{2,3}

¹ School of Civil and Transportation Engineering, Guangdong University of Technology, Guangzhou 510006, China

² Centre Borelli, ENS-University of Paris-Saclay, 91190 Gif-sur-Yvette, France

³ UTBM, IRAMAT UMR 70 65-CNRS, Rue de Leupe, CEDEX, 90010 Belfort, France

Received: 19 January 2024 / Accepted: 14 May 2024

Abstract. To solve the problems of difficulty in deploying accelerometers in traditional cable force measurement, this paper proposes a cable force measurement method based on unmanned aerial vehicles (UAVs). This method first uses the Kanade-Lucas-Tomasi (KLT) optical flow method to track the vibration video of the bridge cable target points captured by the UAV, obtaining its displacement-time-history curve. Then, the empirical mode decomposition (EMD) is used to correct these curves to obtain the true displacement response of the target points. Finally, the operational modal analysis (OMA) is used to obtain the natural frequency of the cable from the displacement response, and the cable force is calculated accordingly. The experimental results show that the relative deviation of the measured natural frequency of the cable is within 5% compared with fixed cameras and accelerometers, indicating that the UAV can effectively obtain the natural frequency of the bridge cable and calculate the cable force.

Keywords: Cable force measurement / EMD / KLT-optical flow method / OMA / UAVs

1 Introduction

Monitoring of cable forces in cable-stayed bridges is a vital component of Structural Health Monitoring (SHM). Due to the potential for cable relaxation or damage during operation, resulting in stress loss, there can be adverse effects on the overall structure. In severe cases, this can lead to the collapse of the entire bridge. Therefore, to ensure the safety and prolong the service life of cable-stayed bridge structures during their operational lifespan, it is necessary to perform real-time measurements of cable forces under working conditions [1] to ensure that the cables are under normal load conditions.

Vibration frequency analysis [2,3] is commonly used for cable force measurement. In this method, vibration measurement technique is used to record the dynamic response signals of cables under external excitation. Modal analysis of the response signals is then performed to determine the natural frequencies of the cables, thereby determining the cable forces. Methods for measuring bridge cable response signals can be categorized into contact and non-contact methods. Sensors [4,5] and accelerometers [6] are commonly used tools in contact measurement methods, where these instruments are installed on the surface of bridge cables to obtain structural response signals.

However, this approach can be relatively time-consuming and expensive due to extensive wiring and data acquisition challenges, and manual sensor installation carries a certain level of risk. To overcome the aforementioned drawbacks of contact measurements, non-contact methods such as the global positioning system (GPS) [7] and laser doppler vibrometers (LDVs) [8] have gained popularity. However, these methods also exhibit disadvantages, including high measurement costs, time consumption, and low accuracy. With advances in measurement technology, GPS and LDVs are gradually being replaced by computer vision methods [9,10], which offer higher accuracy and lower cost. Two commonly used computer vision measurement methods are digital image correlation (DIC) [11,12] and optical flow methods [13,14]. In these methods, targets are tracked in videos of vibrating structures to obtain displacement response signals. Modal analysis is then applied to solve for modal parameters such as natural frequencies and mode shapes. Due to the error caused by pixel interpolation [15], the measurement accuracy of DIC technique is limited. Optical flow, as another computer vision measurement method, is proven to be accurate in the application of bridge vibration measurement [16,17]. The KLT optical flow technique [18,19] is an improved variant of the optical flow technique. This method can obtain motion information of target points by using inter-frame displacement of pixel points in successive frames in video under the condition of large pixel displacement between

* e-mail: gongfa.chen@gdut.edu.cn

two frames, thus achieving target tracking. Dong et al. [20] use optical flow for multi-point displacement measurement of structures, while Yan et al. [21] obtain bridge displacement signals from videos using the KLT optical flow method. Traditional computer vision-based measurement methods often use fixed cameras placed near the bridge structure for measurements. However, in certain measurement environments, such as over water or over valleys, it can be difficult to find suitable locations for fixed cameras. Therefore, the use of more flexible UAVs equipped with high-definition cameras [22–26] receives increasing attention for cable force measurement.

During the video recording process, the unstable motions of the UAV [27,28] result in measured displacement signals that not only include the true displacement of the bridge cables but also incorporate false displacements caused by UAV ego-motion. Therefore, to obtain the true displacement response of the bridge cables, it is necessary to correct the displacement-time-history curves obtained by target tracking. Homography transformations [15] and three-dimensional reconstructions [29] require reference points for displacement correction, which may be limited in practical measurements. Hoskere et al. [30] proposed a high-pass filtering technique, to remove the low-frequency noise generated by UAV hovering, but this approach is only suitable when the structural natural frequencies significantly exceed that of the UAV hover noise (about 0.5 Hz). The Fourier transform (FT) and inverse Fourier transform (IFT) filters can effectively filter out low-frequency noise [31,32]. However, this method becomes challenging without prior knowledge of the structural natural frequencies, making it difficult to determine the optimal values for low-frequency signal removal. Tian et al. [33] use the relative displacement between adjacent points on cables to mitigate UAV interference by obtaining cable displacement-time-history curve. However, this method does not account for displacement variations induced by UAV rotation, so it cannot directly represent the true cable displacement signals using the relative displacement of adjacent points between two image frames. EMD technique [34] enables the decomposition of bridge cable vibration displacement signals collected by UAVs without the need for reference points. By analyzing each component of the decomposition, the true displacement signal of bridge cable vibration can be effectively preserved. Yan et al. [21] proposed the use of EMD to correct vibration signals measured by UAVs. Chen et al. [35] applied EMD technique to identify the natural frequencies and modal damping ratios of the Qingma Bridge.

After obtaining displacement responses, modal analysis is performed to determine the natural frequencies of the structure. OMA [36–38] can identify the natural frequencies of a structure using power spectral density (PSD) without the need for direct measurements of the input excitation forces. Sun et al. [39] used a peak-picking method from the PSD curve to identify structural modal parameters under environmental excitation. Once the natural frequencies of the cables are determined, the cable forces can be calculated using the equations of vibration theory [40].

This paper presents a novel cable force measurement method using UAVs. First, the UAV captures videos of bridge cable vibrations. Then, the KLT-optical flow technique is used to track target points on the bridge cables and extract their dynamic displacements. The EMD technique is then applied to eliminate the false displacements induced by the UAV during the data acquisition process to obtain the true cable vibration responses. Finally, OMA is used to process the displacement responses by extracting the natural frequencies of the bridge cables, and the cable forces are calculated using the equations of vibration theory. Through both model experiments and field experiments, the measurements obtained using UAVs are compared with those obtained using fixed cameras and accelerometers to verify the reliability of this method. The novelty of this paper lies in the combination of UAV and the EMD technique, resulting in a new cable force measurement method that provides fast and cost-effective cable force measurement.

2 Methods

As shown in Figure 1, In this study, a fixed camera and a UAV were first used to capture videos of cable vibration excited by a force hammer. The KLT optical flow technique tracked pre-arranged target points on the bridge cable, capturing their position information in each frame. This information was then concatenated to form a displacement-time-history curve (uncorrected displacement signal) for each point. The EMD technique was applied to decompose the displacement-time-history curve into multiple Intrinsic Mode Functions (IMFs) and a residue. The true vibration signals of the cable were determined by modal analysis of these IMF components. OMA was used to process the true vibration signals to obtain the PSD curve of the target point. Finally, the natural frequencies of the bridge cable were extracted from the PSD curve using the peak extraction method, and the cable force value was obtained based on the cable vibration theory. The technical flowchart of this paper was as follows:

2.1 KLT optical-flow method

Optical flow was a method that used the changes in pixel intensity over time in an image sequence, and the correlation between adjacent frames, to establish the correspondence between the current frame and the previous frame, and thereby calculated the motion information of objects between adjacent frames. Optical flow referred to the instantaneous velocity of a spatially moving object in the image plane. By calculating the inter-frame displacement of the target point at all vibration times, the displacement-time-history curve of the target point during this time could be obtained.

KLT optical flow method was an optical flow method that had similar assumptions to the basic optical flow methods, it must satisfy:

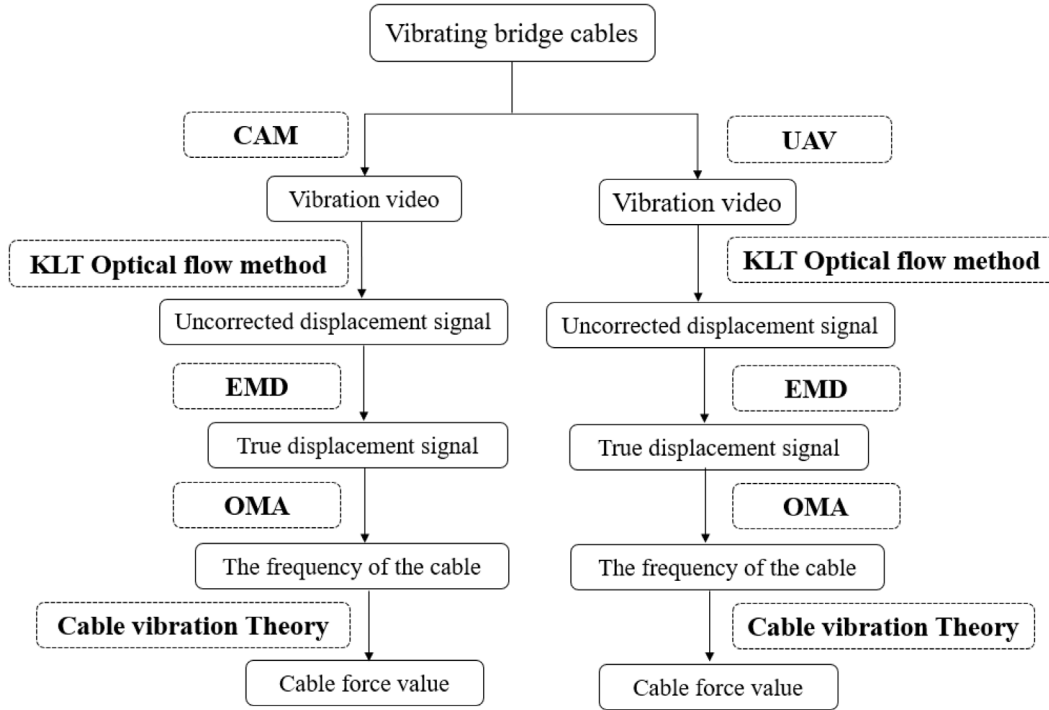


Fig. 1. Technical flowchart. Note: CAM indicates fixed camera.

- Brightness constancy: the pixel values of the image did not change between frames to ensure that target tracking was not affected by brightness.
- Temporal continuity or small motion of the target point: each pixel in the image undergoes only small motion to ensure that the KLT algorithm could track the target point.
- Spatial consistency, neighboring points had similar motion: within a small fixed-size window, the offset of all points was the same.

As shown in Figure 2, I_1 was the first frame image, I_2 was the current image; (x, y) was the coordinate of the target point, $\mathbf{X}=[x, y]^T$, in the first image, while $(\mathbf{X}+\mathbf{d})$, represented the point with the offset vector, $\mathbf{d}=[d_x, d_y]^T$, from the target point, here d_x and d_y were coordinates of the offset vector. While W was the fixed-size window centered on the concerned point, the residual calculation of the window centered on the target point with that centered on the point, $(\mathbf{X}+\mathbf{d})$, in the current image was:

$$\varepsilon = \iint_W [I_2(\mathbf{X}+\mathbf{d}) - I_1(\mathbf{X})]^2 d\mathbf{X}. \quad (1)$$

By solving the minimization of equation (1), the coordinates of the target point in each frame of the video could be obtained. By connecting the coordinates of the target point in each frame over the measurement time period, the displacement-time curve for that target point could be obtained.

2.2 Empirical mode decomposition

During the shooting process of a UAV over a bridge, the collected displacement-time-curve (original vibration-displacement signal) contained false displacements caused by UAV ego-motion [41]. Therefore, eliminating the false displacement caused by the UAV was an important aspect. In this paper, the EMD was used to decompose the vibration signals collected by the UAV, and the noise signal was eliminated by analyzing the PSD curve of each signal component after decomposition, and then the true displacement signal of cable vibration was obtained.

The EMD method was a non-stationary signal analysis method. The EMD process sequentially decomposed fluctuations and trends of varying scales in the signal, resulting in data sequences of distinct characteristic scales known as IMFs. Each IMF needed to meet two specific conditions:

- Throughout the time domain, the number of local zero points and extrema point of each IMF component were equal or differ by no more than 1.
- At any given moment, the mean value of the upper envelope, formed by the local maxima, and the lower envelope, formed by the local minima, equaled zero, which meant that the upper and lower envelope lines displayed local symmetry regarding the time axis.

By iteratively decomposing the original signal $x(t)$ through the EMD, n IMFs and residual $r_n(t)$ could be obtained:

$$x(t) = \sum_{i=1}^n I_i(t) + r_n(t), \quad (2)$$

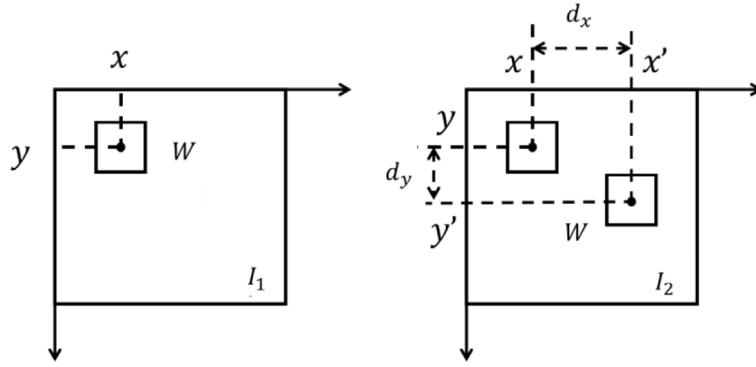


Fig. 2. Schematic diagram of optical flow method.

where $I_i(t)$ was the decomposed signal components, and n was the number of *IMFs*.

The EMD decomposition process of complex signal $x(t)$ was as follows:

Step 1:

First, all the extreme points of the signal $x(t)$ were found. Then, all the local maximum points were connected to form the upper envelope e_{\max} , and all the local minimum points were connected to form the lower envelope e_{\min} . The mean envelope $m_1(t)$ was obtained by calculating the average of the upper and lower envelope:

$$m_1(t) = \frac{e_{\max}(t) + e_{\min}(t)}{2}. \quad (3)$$

Step 2:

The intermediate signal $C_{1,1}(t)$ was obtained by subtracting the mean envelope from the original signal:

$$C_{1,1}(t) = x(t) - m_1(t). \quad (4)$$

If the intermediate signal $C_{1,1}(t)$ satisfied the two conditions of *IMFs* mentioned above, then it was an *IMF* component $I_1(t)$; if it did not satisfy the requirements, starting with signal $C_{1,1}(t)$ as the original signal, calculated its mean envelope $m_1(t)$. Then, subtracted $m_1(t)$ from $C_{1,1}(t)$ to obtain a new intermediate signal $C'_{1,1}(t)$. Determined whether $C'_{1,1}(t)$ satisfied the two conditions mentioned for *IMF*. If it did, then $C'_{1,1}(t)$ became the first *IMF* component, denoted as $I_1(t)$.

Step 3:

$I_1(t)$ represents the high-frequency *IMF* component in the original signal $x(t)$. The remaining component $r_1(t)$ was obtained by subtracting $I_1(t)$ from the original signal $x(t)$. The second *IMF* component $I_2(t)$ was obtained by performing the above screening process on $r_1(t)$. That is, starting with signal $r_1(t)$ as the original signal, calculated its mean envelope $m_1(t)$. Then, subtracted $m_1(t)$ from $r_1(t)$ to obtain an intermediate signal. If this intermediate signal satisfied the two conditions mentioned for *IMF*, then it became the second *IMF* component, denoted as $I_2(t)$. The remaining component $r_2(t)$ was obtained by subtracting $I_2(t)$ from $r_1(t)$, until the last residual signal $r_n(t)$ could not be further decomposed, which meant that if the residual signal $r_n(t)$ was a monotone function, then the

decomposition of signal $x(t)$ was completed.

$$x(t) - I_1(t) = r_1(t) \quad (5)$$

$$r_1(t) - I_2(t) = r_2(t) \quad (6)$$

$$r_{n-1}(t) - I_n(t) = r_n(t). \quad (7)$$

Thus, the sum of all *IMF* components and residual component $r_n(t)$ was the original signal $x(t)$, which was listed in formula (2).

2.3 Operational modal analysis and cable force calculation

After obtaining the response signal of the bridge cable, modal analysis was required to obtain modal parameters. *OMA* used only the response signal. There were two commonly used transfer ratio methods: the response signal-based transfer ratio and the *PSD*-based transfer ratio, which could be used to obtain the modal parameters of the structure. In a multi-degree-of-freedom system, the expression of the response transfer ratio $T_{io}(\omega)$ was [42]:

$$T_{io}(\omega) = \frac{X_i(\omega)}{X_o(\omega)}, \quad (8)$$

where $X_i(\omega)$ and $X_o(\omega)$ represented the *FT* of the displacement responses $x_i(t)$ and $x_o(t)$ at degrees of freedom i and o , respectively. The expression of *PSD* transfer ratio $\hat{T}_{io}(\omega)$ was [37]:

$$\hat{T}_{io}(\omega) = \frac{s_{i,o}(\omega)}{s_{o,o}(\omega)} = \frac{X_i(\omega)X_o^*(\omega)}{X_o(\omega)X_o^*(\omega)} = T_{io}(\omega), \quad (9)$$

where $s_{i,o}(\omega)$ was the cross *PSD* of the displacement responses $x_i(t)$ and $x_o(t)$; $s_{o,o}(\omega)$ was the self-*PSD* of displacement response $x_o(t)$; $X_o^*(\omega)$ was the conjugate complex of $X_o(\omega)$.

According to the principle of dynamics, the energy of the displacement response was higher at the natural frequency. Therefore, a peak would appear on the *PSD* curve at the structure's natural frequency, and the peak

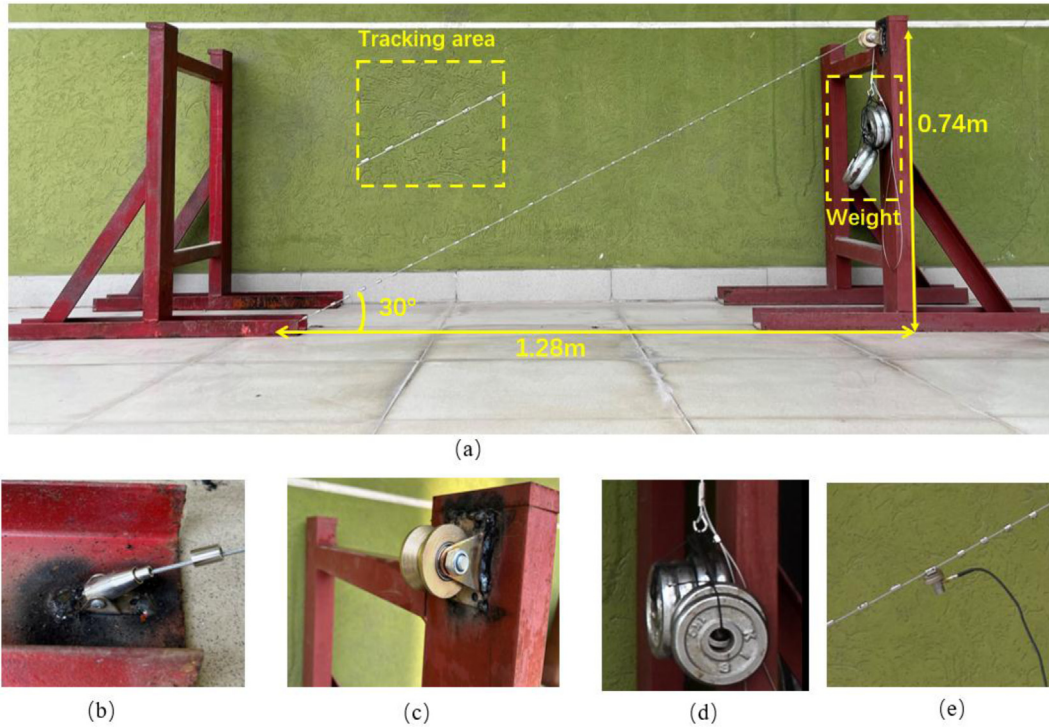


Fig. 3. Experimental model: (a) Experimental model; (b) Cable base; (c) Fixed pulley; (d) Weight; (e) Cable.

value of the PSD curve for any degree of freedom was taken as the cable's natural frequency. Since it had been proved and extracted in previous works that a UAV could obtain the modal parameters of bridge structures [43], this paper only measured a target point on the cable to obtain its displacement and natural frequency.

The vibration frequency method of measuring cable force was obtained by measuring the natural frequency of the cable and assuming that the cable was fixed at both ends without considering the bending rigidity of the cable. The calculation formula was:

$$T = \frac{4ml^2 f_n^2}{n^2}, \quad (10)$$

where T was the cable force, f_n was the n th order natural frequency of the cable, l was the cable length, m was the mass per unit length of the cable.

To accurately measure cable force, factors such as boundary conditions at both ends of the cable, cable bending stiffness, sag, inclination, length, etc. must be considered. These factors were discussed in the discussion section of this article.

3 Experiment

3.1 Experimental validation

3.1.1 Experimental set-ups and instruments

The experimental model (Fig. 3) consisted of a fixed steel frame (a), a cable base (b), a cable (e), a fixed pulley (c), and a weight (d); the steel frame was 74 mm high and the horizontal distance between the cable base and the pulley was 128 mm; the cable base and the pulley were welded to

the steel frame. The cable was a 2 mm plastic-coated steel wire rope, which was fixed at the cable base at one end and connected at the other end to a counterweight over a hook.

The video of cable vibration was captured by a fixed camera (D5300, Nikon Corporation, Tokyo, Japan) in Figure 4a and a quadcopter UAV (Mavic Air 2, DJ-Innovations, Shenzhen, China) in Figure 4b. The acquisition frequency of the fixed camera was 50 frames/second and the acquisition frequency of the UAV was 30 frames/second. During the acquisition, the cable was properly excited using a force hammer as shown in Figure 4c, and the fixed camera and UAV were each placed two meters away from the cable for acquisition [43].

To validate the effectiveness of the optical measurement method, a dynamic signal acquisition instrument (JM3840, Jing-Ming Technology Inc., Yangzhou, China) (Fig. 4d) and an accelerometer sensor (YD2150, Jing-Ming Technology Inc., Yangzhou, China) (Fig. 4e) were used. In addition, a computer (ThinkPad E570, Lenovo, Beijing, China) (Fig. 4f) was used to connect the data acquisition systems to retrieve the vibration signals from the cables. The acceleration signal collected by the accelerometer was used as the reference. The signal acquisition instrument had a sampling frequency of 2 kHz, and the accelerometer had a sampling frequency range of 0.5–8 kHz. The computer configuration included CPU: Intel Core i5-7200U (2.50 GHz) and 16 GB of memory (2133 MHz).

3.1.2 Experimental scheme

The present study validated the proposed measurement method based on UAVs and EMD for accurately tracking the displacement and obtaining the modal parameters of the cable through experiment. The experimental layout

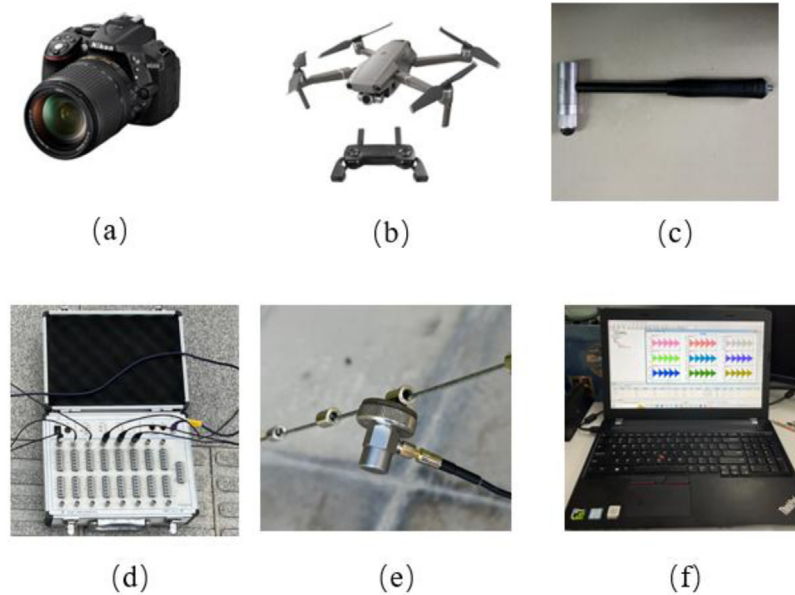


Fig. 4. Experimental instruments: (a) Fixed camera; (b) DJI UAV; (c) A force hammer; (d) Dynamic signal acquisition instrument; (e) Accelerometer; (f) Computer.

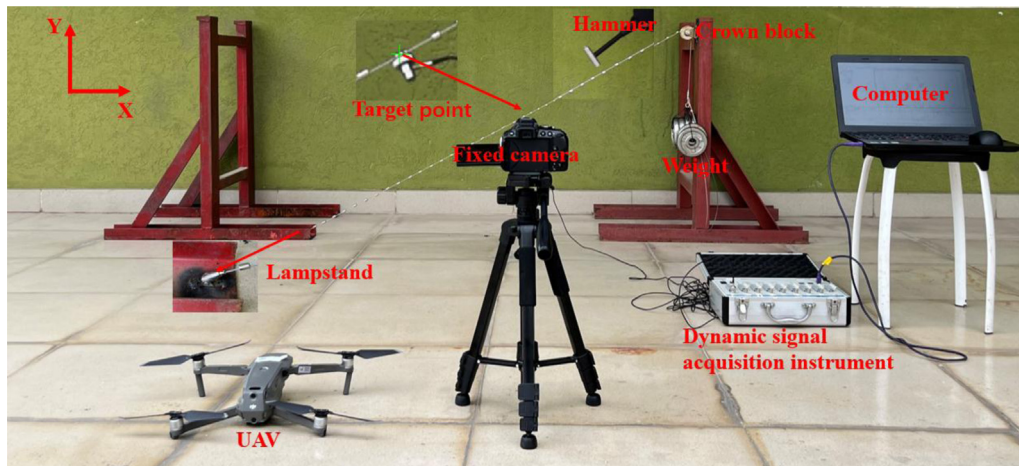


Fig. 5. Experimental layout.

was labeled in Figure 5, where the displacement signal of the target point was captured using both a fixed camera and a UAV. During the collection process, the cable was excited by five times. The excitation interval was 4 seconds, the acquisition time was 20 seconds [44], while the acceleration signal was collected by a dynamic signal acquisition instrument to ensure the synchronization of the acquisition time.

3.1.3 Experimental results and analysis

The analysis of the experimental results was mainly divided into two parts:

- The displacement-time-history curves collected by the UAV were corrected using the EMD and FT methods, with the fixed camera serving as a reference. The degree of burrs in the corrected acceleration signal and the

relative error of the natural frequency of the cable were used as indicators to evaluate the effectiveness of the two correction methods.

- The accelerometer was used as a reference, the EMD method was used to correct the displacement-time-history curves from both the fixed camera and the UAV, and a comparison of the natural frequencies obtained from the three measurement methods was conducted. The relative error of the natural frequencies obtained from the three methods was used as an indicator to verify the feasibility and accuracy of using UAVs for cable vibration measurement.

Due to the use of a force hammer to excite the cable in the Y-direction in the experiment, the displacement of the cable in the Y-direction was relatively large. In order to better observe the amplitude, this paper only considered the vertical displacement of the target points tracked by

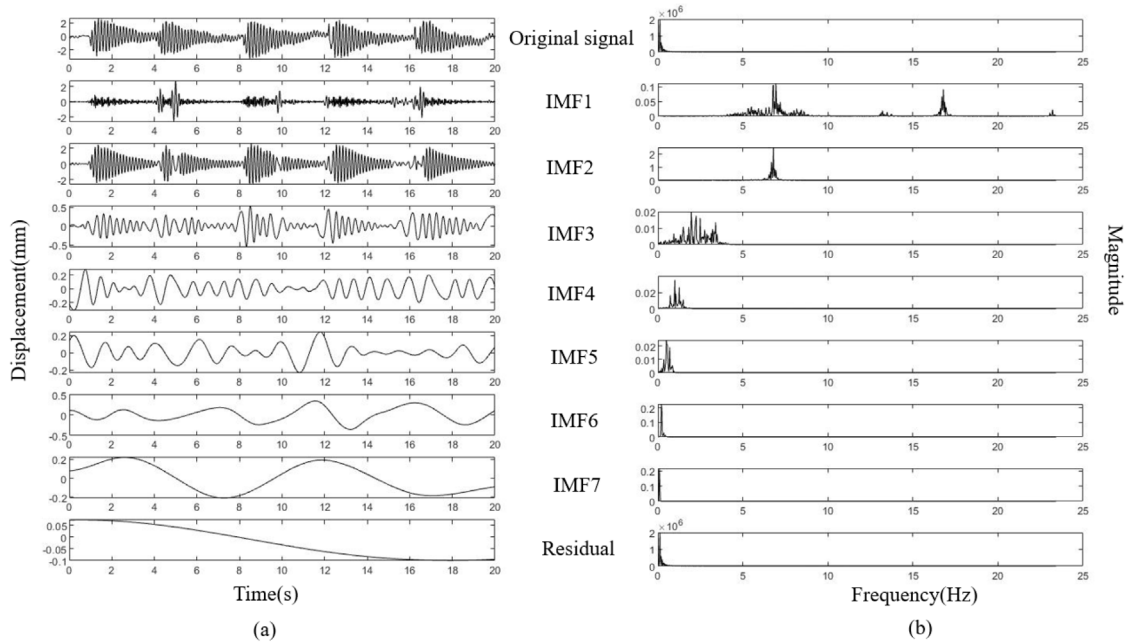


Fig. 6. (a) EMD decomposition of fixed camera displacement-time-history curve; (b) PSD curve of each mode component of fixed camera.

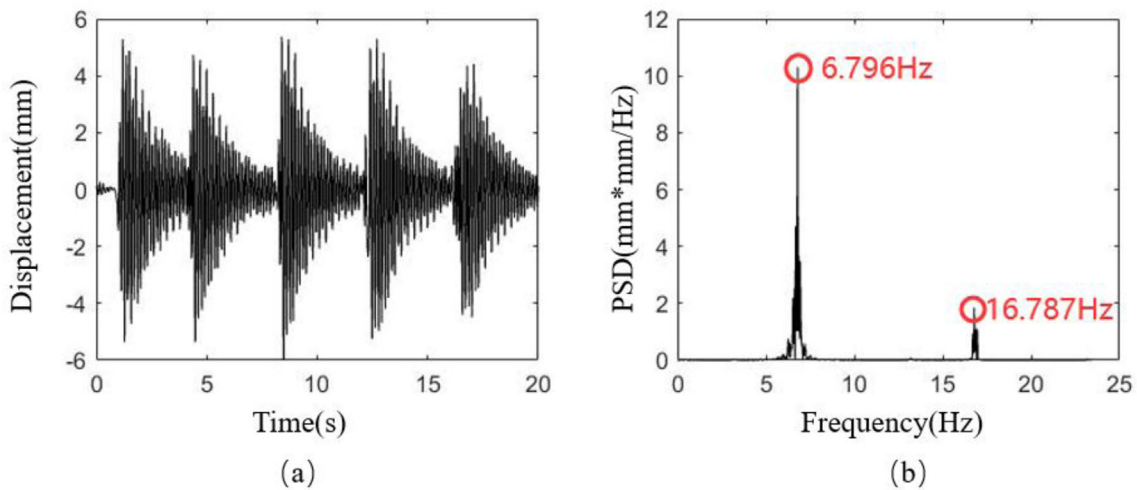


Fig. 7. (a) Fixed camera IMF12 displacement-time-history curve; (b) Fixed camera IMF12 PSD curve.

the fixed camera and UAV. As shown in Figure 6, the original displacement-time-history signal tracked by the fixed camera had a significant peak at 0 Hz, which overshadowed the true natural frequency of the cable, so it needed to be corrected to extract the true vibration signals of the cable model.

The original vibration signals acquired by the fixed camera were decomposed by the EMD. As shown in Figure 6a, the original vibration signal was decomposed into 7 IMF components and 1 residue, which represented different frequency components (in the order from high to low). The first and second IMFs had the decaying characteristics of free vibration, and the residue after decomposition was monotonic, which was the condition

for terminating the EMD process. The IMFs and residue were analyzed separately. As shown in Figure 6b, except for the first and second IMFs, the peaks of the PSD curves of other IMF components were around 0 Hz. According to the OMA theory, the frequency of these IMF components was around 0 Hz. The first and second IMF components were added together to integrate a new signal. IMF12 (Fig. 7a) represented the true displacement signal of the cable after removing the low frequency noise signal. The recombined signal was smoother than the original displacement-time-history curve. The PSD curve was obtained and the peak extraction method was used to obtain the first two natural frequencies, 6.796 Hz and 16.787 Hz, respectively.

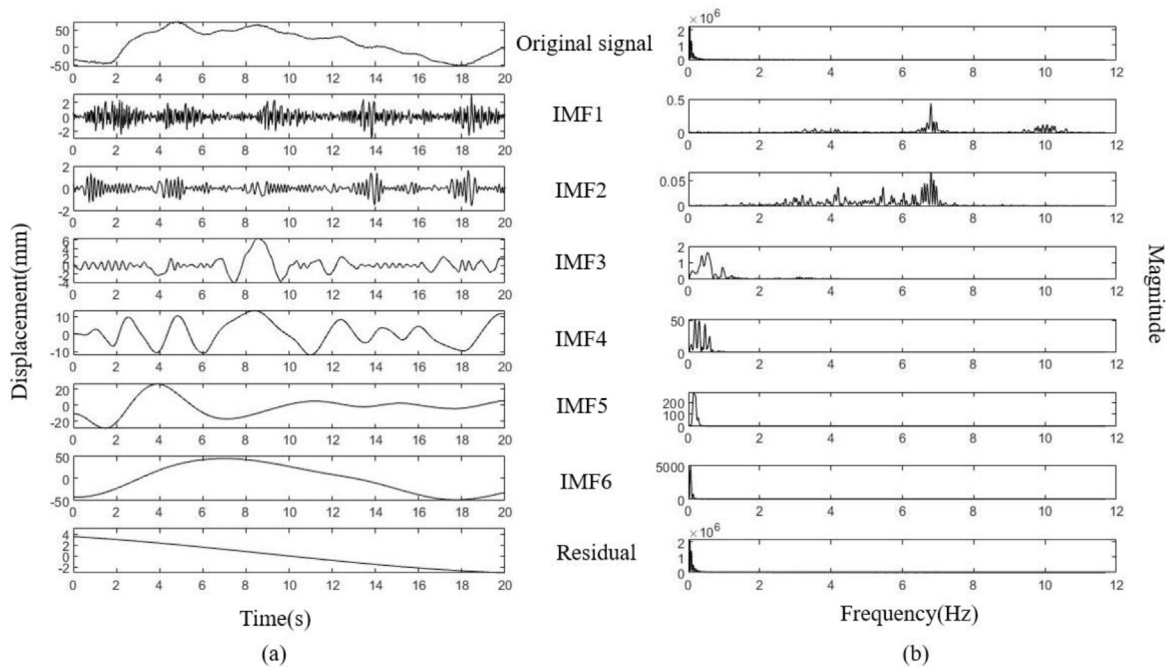


Fig. 8. (a) EMD decomposition of UAV displacement-time-history curve; (b) PSD curve of each mode component of UAV.

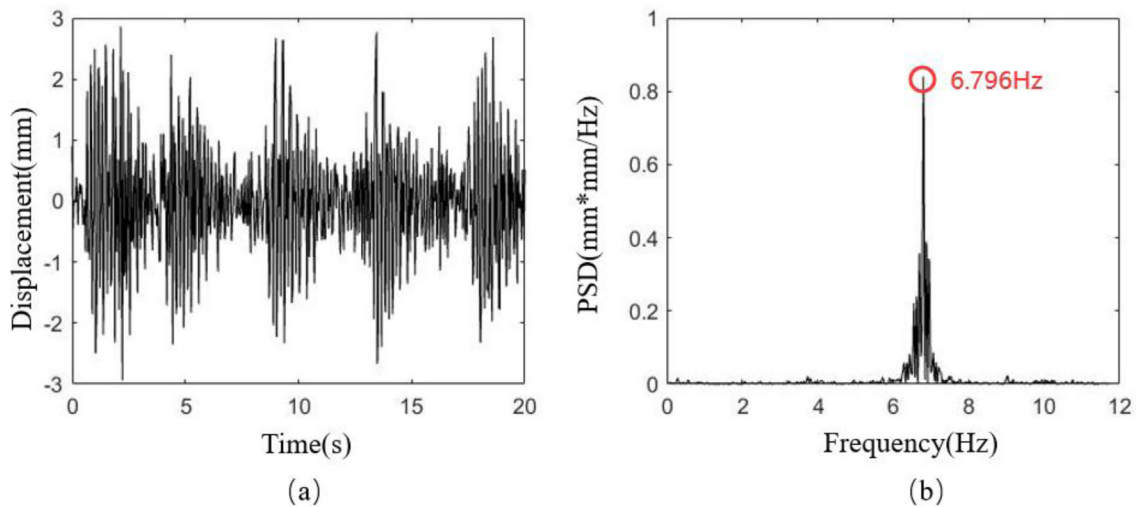


Fig. 9. (a) UAV IMF12 displacement-time-history curve; (b) UAV IMF12 PSD curve.

Similarly, the displacement-time-history signal collected by the UAV exhibited significant drift due to UAV ego-motion and environmental influences (Fig. 8). The PSD curve of the original displacement signal collected by the UAV showed a significant peak at 0 Hz, which was caused by false signal. Therefore, the original signal must be corrected to extract the true displacement signal of the cable-stayed model.

By performing the EMD decomposition on the original displacement signal collected by the UAV (Fig. 8a), the original vibration signal was decomposed into 6 IMF components and 1 residue. The first and second IMFs had the characteristic of free decay, and the decomposed residue was monotonic, which was the termination condition of the EMD process. The PSD curve was

calculated for each IMF component and residue separately (Fig. 8b). Except for the first and second IMFs, the PSD peaks of the other IMF components were close to 0 Hz, which was induced by low-frequency UAV ego-motion. The first and second IMF components were added together to integrate a new signal, and the resulting displacement-time-history curve, IMF12 in Figure 9a, was the true displacement signal of the cable model. After removing the low-frequency noise from the curve, the first-order frequency was obtained as 6.796 Hz by picking the peak from the obtained PSD curve, which was consistent with the frequency obtained by the fixed camera. It also proved that the EMD method could be used to solve the modal parameters of the cable from the displacement signals collected by UAVs.

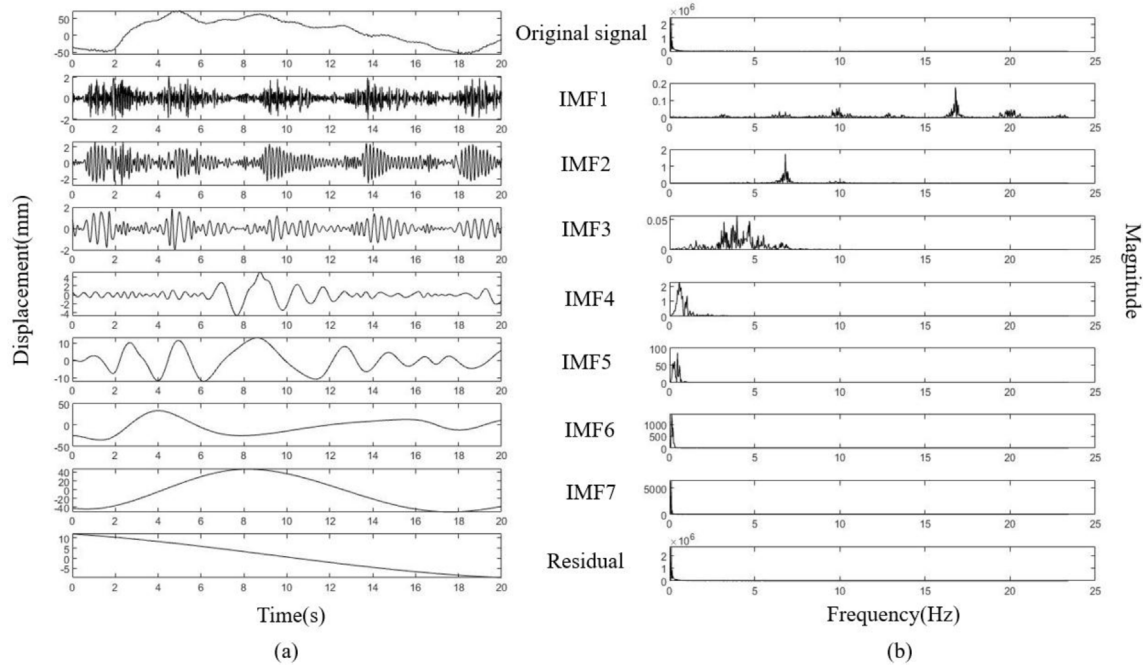


Fig. 10. (a) EMD decomposition of UAV displacement-time-history curve; (b) PSD curve of each mode component of UAV.

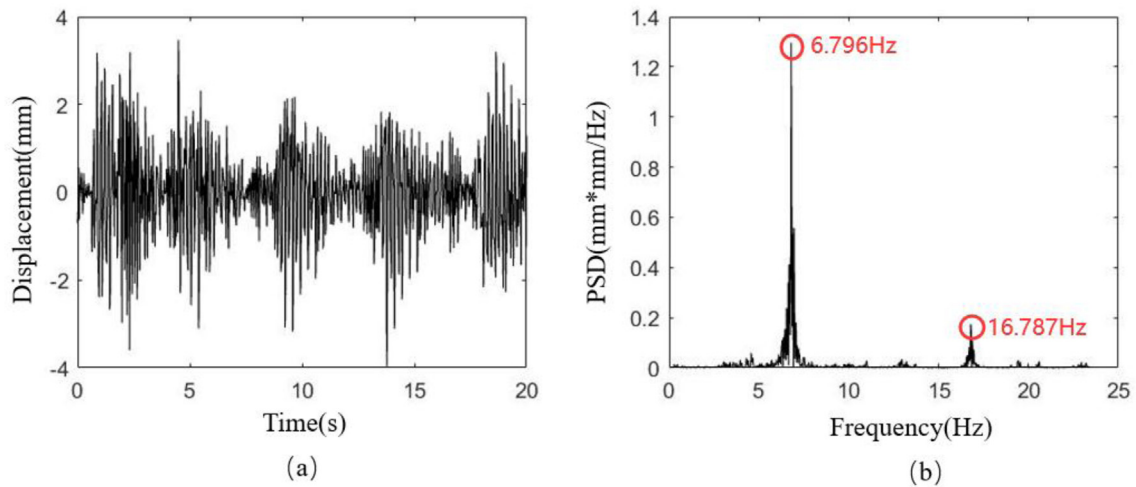


Fig. 11. (a) UAV IMF12 displacement-time-history curve; (b) UAV IMF12 PSD curve.

Compared with the fixed camera, the UAV did not capture the next-order frequency, mainly because the frame rate of video captured by the UAV was 30 frames per second, which means that it could not capture higher order frequencies. To solve this problem, a UAV with a higher frame rate could be used for capturing, or the video captured by the UAV could be output at a higher frame rate using video editing software to increase the sampling frequency, which would be discussed in the following sections. The principle of the relationship between video frame rate and sampling frequency would be explained in detail in the discussion section.

Based on the obtained cable frequency, the cable force could be calculated, which would be discussed in [Section 3.2](#) on the actual bridge cable.

To increase the sampling frequency of the UAV, this paper outputs the video of bridge cable vibration collected by the UAV as 50 frames per second through video editing software. As above, the KLT optical flow technique was first used to track the displacement-time history curve of the video, and then the EMD was used to decompose the displacement-time history curve into 7 IMF components and a residue ([Fig. 10a](#)). By adding IMF1 and IMF2 together, the displacement-time-history curve IMF12

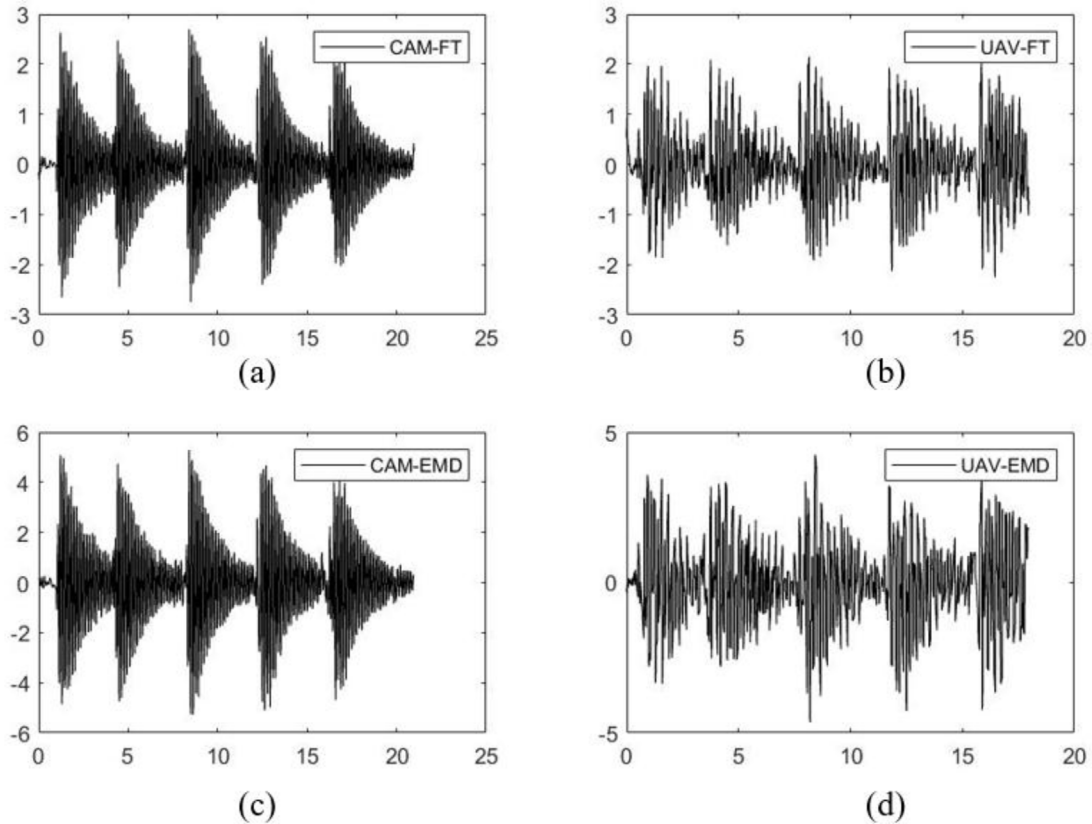


Fig. 12. Displacement-time-history curve after correction under four different conditions: (a) CAM-FT; (b) UAV-FT; (c) CAM-EMD; (d) UAV-EMD. Note: CAM indicates fixed camera; CAM-FT indicates that the signal collected by the fixed camera is corrected by FT method; CAM-EMD indicates that the signal collected by the fixed camera is corrected by EMD method; Other expressions were similar.

(Fig. 11a) was obtained. The PSD curve of this curve was then plotted and the frequencies were extracted using the peak-picking method, which were 6.796 Hz and 16.787 Hz in Figure 11b, these results were consistent with the inherent frequencies obtained from the fixed camera, indicating that increasing the frame rate of the UAV acquisition could effectively improve its sampling frequency. To quantify the measurement displacement error caused by the inherent vibration of the UAV, this paper summed the remaining IMF components (IMF3-Residual) and calculated their average, which was defined as the fluctuation error caused by the vibration of the UAV. According to the experimental data, the fluctuation error caused by the UAV was 3.73 mm.

In order to further verify the effectiveness of the EMD method for decomposing displacement signals collected by UAV, this paper corrected the original displacement signals collected by fixed camera and UAV by a filter composed of FT and IFT, and compared the displacement-time-history curve and PSD curve obtained by the two methods.

Since the vibration frequency of the UAV motion was relatively small compared to the natural frequencies of the cable, a filter combining FT and IFT could be employed to eliminate low-frequency signals: first, the original displacement signal was transformed into a frequency spectrum by FT, and the low-frequency part of the spectrum was

removed [21], and then IFT was used to transform the frequency-domain signal back into a time-domain signal, resulting in the true displacement signal of the cable model.

In this paper, the degree of burr in the displacement-time-history curve was used as an indicator for the evaluation of two methods. The locally weighted regression [45] could be used to smooth the original displacement signal $x(t)$, to obtain the desired displacement-time-history curve $x'(t)$, the level of burr in the curve can be evaluated using the average value of the error curve, denoted as ECA in this study, which represents the deviation between $x(t)$ and $x'(t)$. A higher ECA indicates a greater level of burr in the curve. The results showed that the ECA of the EMD method was lower, 4.121, while the ECA of FT-IFT was 5.467.

Figure 12 showed the displacement-time-history curve of the original signals collected by the fixed camera and the UAV corrected by the EMD and FT-IFT methods, respectively. The corrected signal obtained by FT-IFT and the EMD methods for the original displacement signal recorded by the fixed camera showed an obvious vibration decay trend, and the curve was smoother. While the original displacement signal recorded by the UAV corrected by the above two methods had an obvious vibration decay trend, but there were more burrs. This was due to the ego-motion of the UAV, resulting in obvious drift of the collected original signal. Even after correction, there were still more burrs.

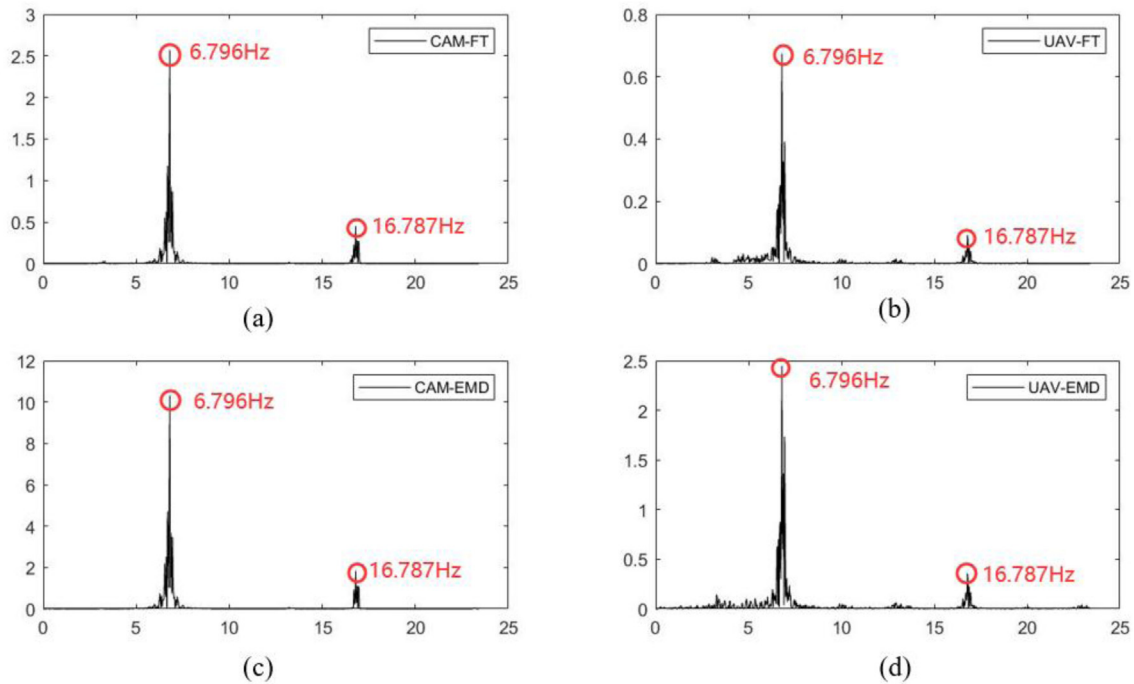


Fig. 13. PSD under four different conditions: (a) CAM-FT; (b) UAV-FT; (c) CAM-EMD; (d) UAV-EMD.

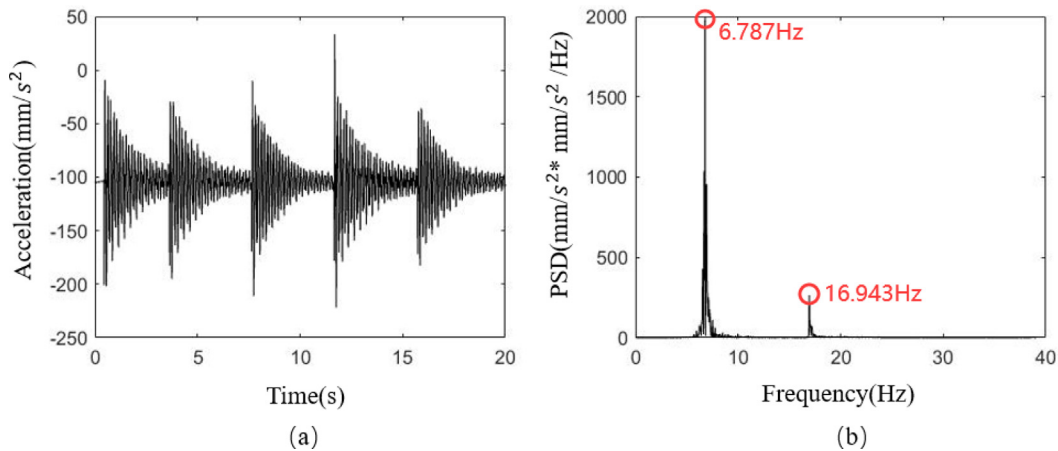


Fig. 14. (a) Acceleration time-history curve; (b) Acceleration PSD curve.

Figure 13 showed the PSD curves obtained from the corrected signals, revealing distinct peaks in both methods, the obtained natural frequencies were found to be consistent, indicating that the two methods had good performance in extracting the natural frequencies of cables.

The filter composed of FT-IFT could effectively remove the low-frequency noise, but it was difficult to determine the optimal value of the filter frequency without prior knowledge of the cable natural frequencies, resulting in difficulty in effectively removing low-frequency signal parts. The EMD method could directly decompose the original signal and determine structure's natural frequency by analyzing the PSD curve of each IMF component. When compared to the FT-IFT method, the EMD method had a lower ECA value, the curve exhibited fewer burrs, and the

extracted natural frequency of the cable model was consistent with the FT-IFT method. In summary, the EMD method was superior to the FT-IFT method in extracting the true displacement signal of the cable.

To further verify the accuracy of the UAV measurement in extracting the natural frequencies of the cable model, this paper compared the relative error in the natural frequencies obtained through the three methods: the accelerometer, the fixed camera, and the UAV, with the accelerometer as the reference. Figure 14a showed the time-history curve of the cable vibration collected by the accelerometer at a sampling frequency of 100 Hz. In the experiment, the cable was excited by five times, and the acceleration signals showed a fifth decay trend. The time-history signal collected by the accelerometer was analyzed

Table 1. The average relative error of natural frequency of the three measurement methods.

Methods	1st (Hz)	2nd (Hz)
ACC	6.771	16.992
CAM	6.792	16.846
Relative error (%)	0.31%	0.86%
UAV	6.798	16.797
Relative error (%)	0.40%	1.15%

Note: ACC indicates accelerometer.

by OMA to obtain its PSD curve (Fig. 14b), and the first two natural frequencies of the cable model were extracted by the peak-picking method, which were 6.787 Hz and 16.943 Hz, respectively. As analyzed before, the natural frequencies of the cable model extracted by the fixed camera and the UAV were both 6.796 Hz and 16.787 Hz, and the relative errors with respect to the natural frequencies extracted by the accelerometer were 0.13% and 0.92%, respectively. This indicated that the UAV combined with the EMD method had high accuracy in extracting the natural frequencies of the cable model.

To reduce the experimental errors, this study conducted three experiments and used the averaging method to increase the reliability of the results [12]. As shown in Table 1, with the accelerometer result as the reference, the average relative errors of the first two natural frequencies of the cable model obtained by the fixed camera in three experiments were 0.31% and 0.86%, respectively, while the UAV were 0.40% and 1.15% respectively. The error accuracy was within 5%. The relative percentage errors for the first two natural frequencies measured by the fixed camera and the UAV were 0.09% and 0.29%, respectively. This further verified that the UAV combined with the EMD method exhibited high accuracy in extracting the natural frequencies of the cable model.

3.2 Field experiment

3.2.1 Overview of bridges

The Conghua Bridge was located on Conghua Avenue, Guangzhou, China, with a total length of 466 m. The main bridge was a 136-meter suspender arch bridge (Fig. 15). There were 13 suspenders for each auxiliary arch, and the specifications of the suspenders were PES(FD)7-73. There were 19 suspenders for the main arch, and the specifications of the suspenders were PES(FD)7-187 (Fig. 16).

3.2.2 Experimental equipment and scheme

The experimental equipment used in this experiment was shown in Figure 17. The video of cable vibration was collected by a fixed camera (Fig. 17a) and a UAV (Fig. 17b). The fixed camera and the UAV were the same as described in Section 3.1. To verify the effectiveness of the optical measurement method, the experiment also simultaneously used a wireless accelerometer (DH5906W, Jiangsu East China Testing Technology Co., Ltd.,

Jingjiang, China) in Figure 17c and a computer (Fig. 17e) to collect the acceleration signal of the cable and the results obtained by the accelerometer were used as a reference. Figure 17d showed the force hammer used to excite the cable. The wireless accelerometer had a sampling frequency of 1 kHz and a frequency response from DC to 120 Hz. The computer configuration was the same as described in Section 3.1.1.

The experimental layout was shown in Figure 18, where the target points and accelerometer were first attached to the cable (Fig. 18a), and the UAV and the fixed camera were positioned at a certain distance from the tested cable (Figs. 18b and 18c) (ensuring that the target points were within the shooting range). The tested cable was the 5th to 8th (N5-N8) on the right side of the bridge, as shown in Figure 19.

The purpose of this experiment was to validate the reliability of using UAVs combined with the EMD method to measure cable forces.

During the experiment, target points were attached to the cables and accelerometers were installed on the cable. The UAV was positioned 2 m away from the target points on the cable, and the fixed camera was positioned 3 m away from the target points (to ensure that the target points were within the camera's shooting range). A force hammer was used to excite the cables while the fixed camera and UAV captured the cable vibration.

3.2.3 Experimental results and analysis

Taking the N7 suspender as an example. Figure 20a showed the vibration signal collected by the accelerometer. By performing OMA on the signal, the PSD curve shown in Figure 20b was obtained. The first 5 natural frequencies of the N7 suspender were obtained as follows: 3.711 Hz, 7.471 Hz, 11.230 Hz, 14.990 Hz, and 18.848 Hz.

The KLT optical flow technique was employed to track the target point on the N7 suspender captured by the fixed camera, and the original displacement-time-history curve shown in Figure 21a was obtained. The curve had obvious drift, which was caused by the vibration of the bridge deck. Therefore, in order to eliminate the false displacement caused by the camera vibration, the original displacement signal must be decomposed by the EMD, and 7 IMF components and a residue were obtained after decomposition. The IMFs and the residue were analyzed separately (Fig. 21b), which indicated that the frequencies of the suspender were mainly contained in the first three IMFs. The signal obtained by adding the first three IMF components was taken as the true vibration signal of the suspender (Fig. 22a). The PSD curve of the true vibration signal was obtained and its peaks were 3.691 Hz, 7.412 Hz, 11.191 Hz, 14.912 Hz, and 18.808 Hz, corresponding to the first five natural frequencies of the N7 suspender. The relative errors with respect to the frequencies measured by the accelerometer were 0.54%, 0.79%, 0.35%, 0.52%, and 0.21%, respectively. This also proved the effectiveness of the EMD method for decomposing the suspender vibration signal.

Similarly, the same analysis was performed on the N7 suspender collected by the UAV: as mentioned in Section 3.1, increasing the frame rate of the video collected



Fig. 15. Conghua Bridge.

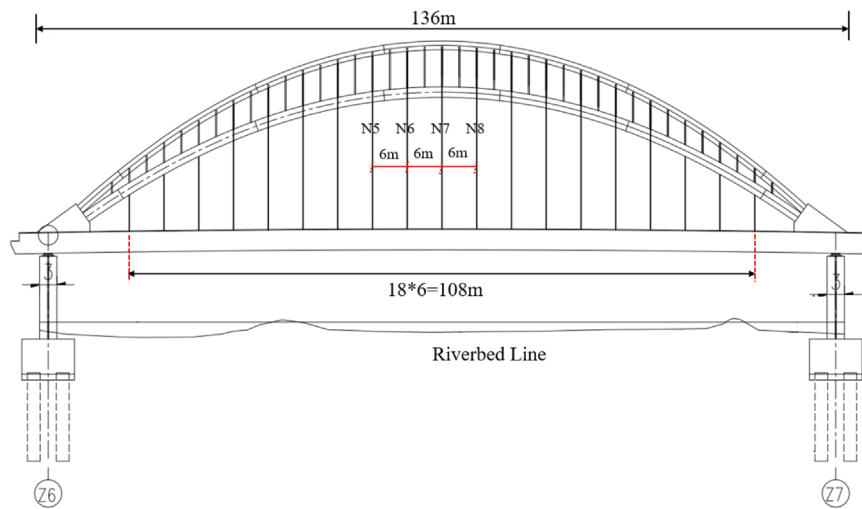


Fig. 16. Layout elevation view of the main bridge type of Conghua Bridge.

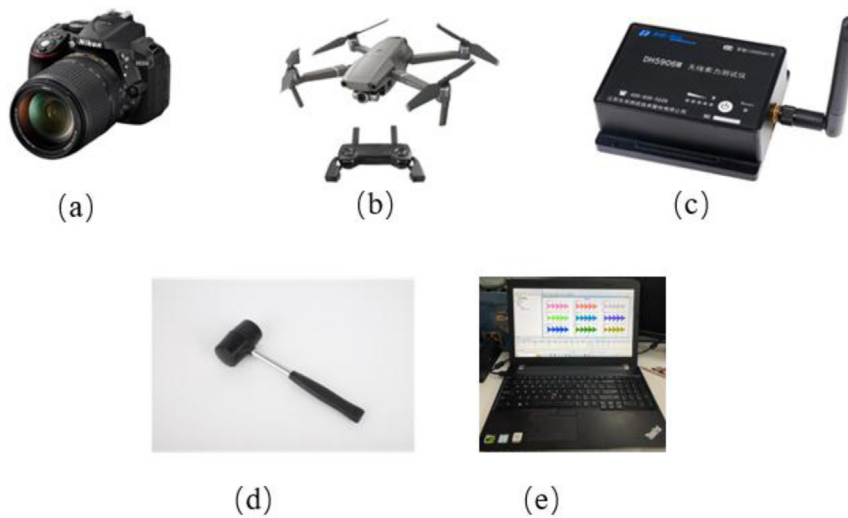


Fig. 17. Experimental instruments: (a) Fixed camera; (b) DJI UAV; (c) Wireless accelerometer; (d) A force hammer; (e) Computer.



Fig. 18. (a) Target point and accelerometer; (b) and (c) Measurement layout of Conghua Bridge.

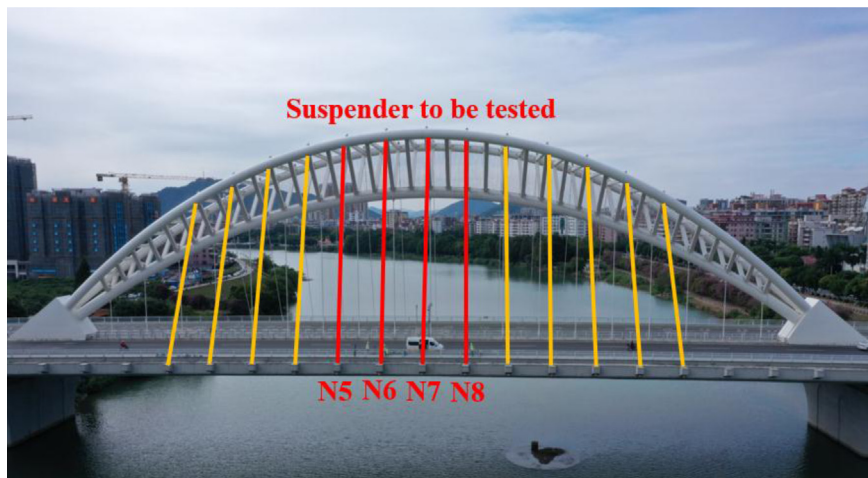


Fig. 19. Suspender to be tested of Conghua Bridge.

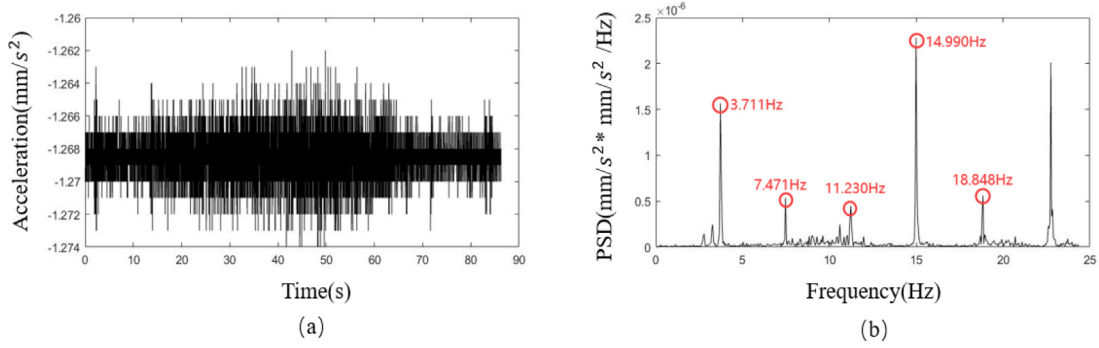


Fig. 20. (a) Acceleration time-history curve; (b) Acceleration PSD curve.

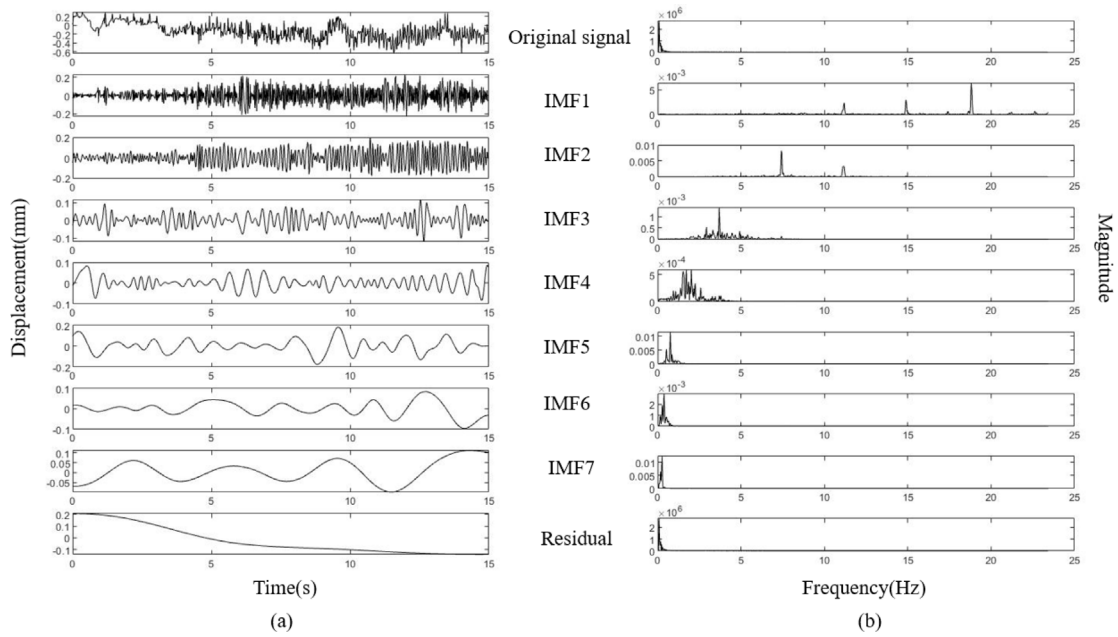


Fig. 21. (a) EMD decomposition of fixed camera displacement-time-history curve; (b) PSD curve of each mode component of fixed camera.

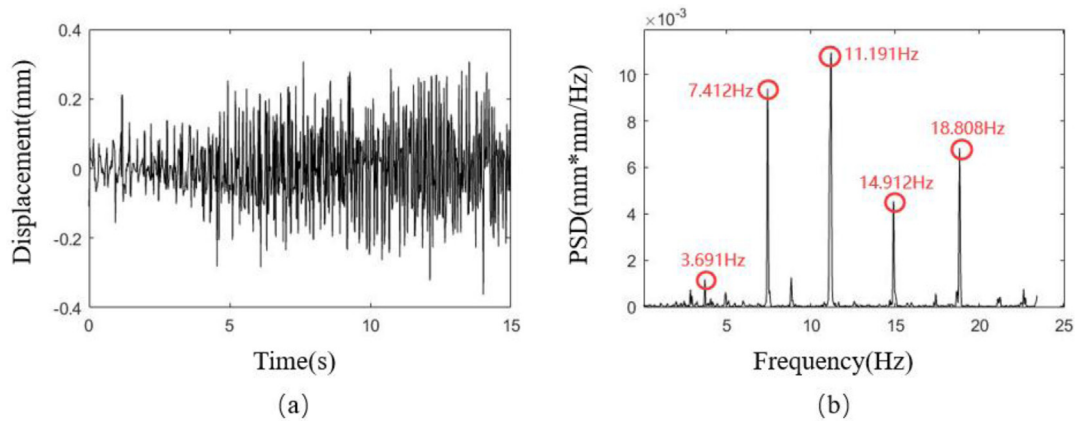


Fig. 22. (a) Fixed camera IMF123 displacement-time-history curve; (b) Fixed camera IMF123 PSD curve.

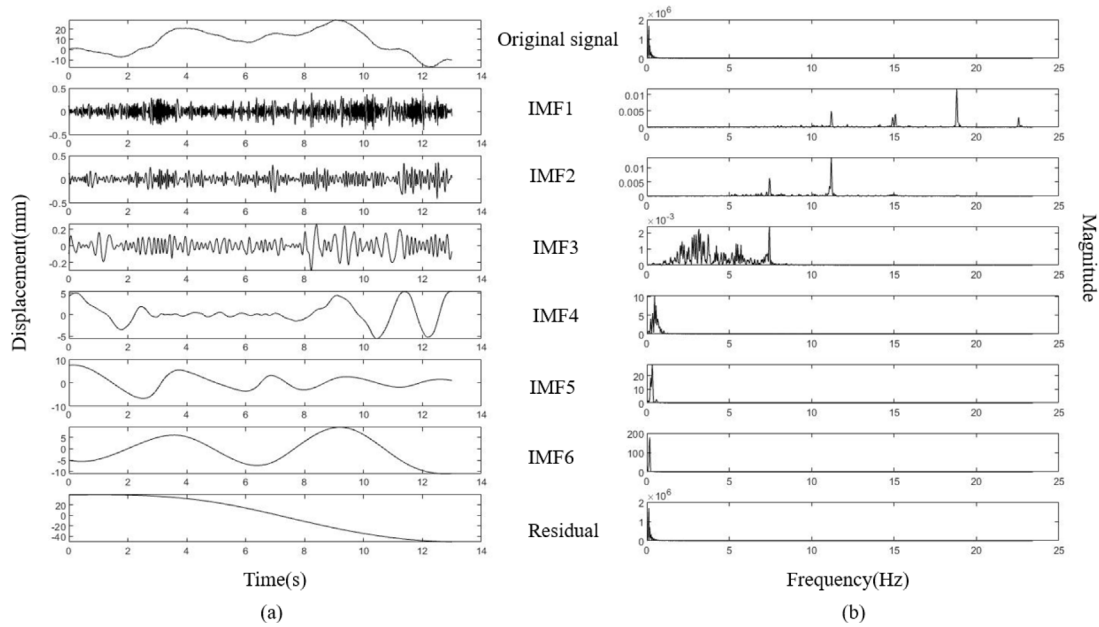


Fig. 23. (a) EMD decomposition of UAV displacement-time-history curve; (b) PSD curve of each mode component of UAV.

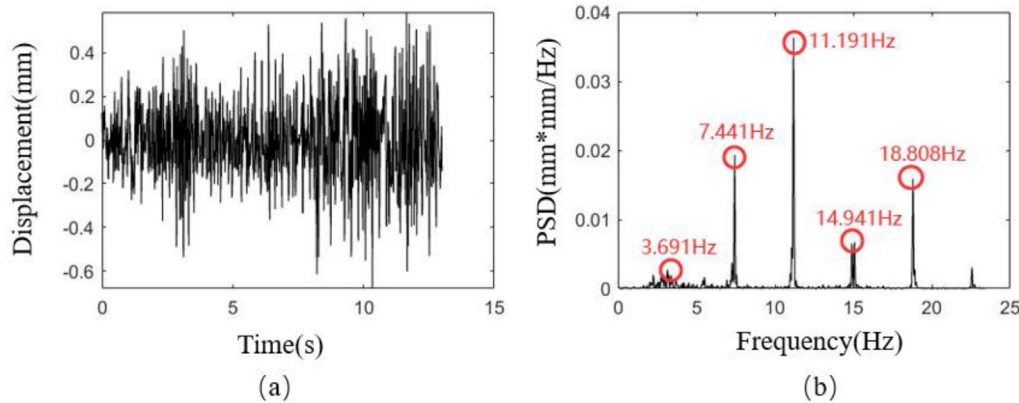


Fig. 24. (a) UAV IMF123 displacement-time-history curve; (b) UAV IMF123 PSD curve.

by the UAV could increase its sampling frequency. Therefore, in this experiment, the video collected by the UAV was first output at 50 frames per second using video editing software. The processed video was tracked using the KLT optical flow technique, resulting in the generation of the original displacement-time-history curve shown in Figure 23a. The curve had a significant drift, which was caused by the internal vibrations of the UAV and the effect of wind disturbances. Therefore, in order to eliminate the false displacement induced by the UAV, the original displacement signal was decomposed by the EMD, resulting in 6 IMF components and the residue. Spectral analysis of these IMF components and residue produced Figure 23b. The figure showed that the frequencies of the suspender were mainly concentrated in the first three IMF components. The signal obtained by adding the first three IMF components was taken as the true vibration signal of the suspender (Fig. 24a). The PSD curve of the true vibration signal was obtained, and its peaks were 3.691 Hz,

7.441 Hz, 11.191 Hz, 14.941 Hz, and 18.808 Hz. The relative errors with respect to the frequencies measured by the accelerometer were 0.54%, 0.40%, 0.35%, 0.33%, and 0.21%, respectively, and the fluctuation error caused by the UAV was 0.94 mm. indicating that the accuracy requirement was met. This also proved the reliability of using the EMD method with UAV to extract the natural frequencies of the suspender.

Table 2 showed the first five frequencies of the four suspenders measured by three measurement methods. The relative errors of the natural frequencies measured by the UAV were within 5% with respect to those measured by the accelerometer and fixed camera, the relative percentage errors for the four natural frequencies of the suspension measured by the fixed camera and the UAV were 2.16%, 1.15%, 0.12%, and 0.07%, respectively. Which further verified the accuracy and reliability of using the UAV in conjunction with the EMD technique for extracting the natural frequencies of the suspenders.

Table 2. Comparison of accelerometer, fixed camera and UAV acquisition frequency.

Suspender number	Measurement method	f1	f2	Frequency (Hz) f3	f4	f5	Mean error (%)
N5	ACC	3.809	7.617	11.475	15.332	19.238	
	CAM	3.779	7.588	11.367	15.264	19.248	
	Relative error (%)	0.79%	0.38%	0.94%	0.44%	0.05%	0.52%
	UAV	3.645	7.617	11.367	14.707	18.633	
	Relative error (%)	4.31%	0%	0.94%	4.08%	3.14%	2.49%
N6	ACC	3.809	7.568	11.377	15.186	19.189	
	CAM	3.809	7.588	11.338	15.234	19.072	
	Relative error (%)	0%	0.26%	0.34%	0.32%	0.61%	0.31%
	UAV	/	7.676	11.338	14.736	19.102	
	Relative error (%)	/	1.43%	0.34%	3.27%	0.45%	1.37%
N7	ACC	3.711	7.471	11.230	14.990	18.848	
	CAM	3.691	7.412	11.191	14.912	18.808	
	Relative error (%)	0.54%	0.79%	0.35%	0.52%	0.21%	0.48%
	UAV	3.691	7.441	11.191	14.941	18.808	
	Relative error (%)	0.54%	0.40%	0.35%	0.33%	0.21%	0.37%
N8	ACC	3.711	7.471	11.279	14.990	18.799	
	CAM	3.712	7.441	11.191	14.971	18.809	
	Relative error (%)	0.03%	0.40%	0.78%	0.13%	0.15%	0.3%
	UAV	3.712	7.441	11.191	14.941	18.779	
	Relative error (%)	0.03%	0.40%	0.78%	0.33%	0%	0.31%

Table 3. Test suspender parameters.

Suspender number	Length (m)	Linear density (kg/m)
N5	32.13	22.1
N6	30.35	22.1
N7	28.28	22.1
N8	30.35	22.1

After obtaining the natural frequencies of the suspenders, the first five frequencies were used in equation (10) to calculate the force values for each suspender. The average of the five force values obtained for each suspender was taken as the final force value. Table 3 showed the calculated length and linear density of the four suspenders.

As shown in Table 4, the relative errors of the force values measured by the UAV and accelerometer were both within 5%, and they were basically consistent with those measured by the fixed camera. This verified the reliability of the UAV in measuring force value.

4 Discussion and conclusions

4.1 Discussion

Although the method proposed in this article could obtain the natural frequencies of the cable and then calculate its cable force value through the cable vibration theory, there were still some problems that needed to be addressed, including:

- About obtaining the target point of a cable. The optical flow method required the target points distinguishable from the background. As the target points were attached to the cables, which was somewhat dangerous. In the future, a spraying UAV could be used to spray colored pigment on the cable to achieve evident targets.
- About the frame rate of UAV acquisition. Due to the limited acquisition frequency of the UAV, it could not acquire the high-order natural frequencies of the cable. In the future, higher frame rate UAVs could be considered to improve the frequency collection range. As shown in Section 3.1 by increasing the output frame rate of the UAV, its sampling frequency could be increased to obtain a higher frequency range. In this article, the frame rate of the video collected by the UAV was given as 50 frames per second, which corresponded to the fixed camera frame rate to ensure consistency of the frequency range. However, it was not necessarily true that the higher the frame rate, the better the results. First, low-frame-rate video could only be increased so much due to software limitations. Second, if the increased frame rate were too different from the original video frame rate, it might cause the structural natural frequency obtained by modal analysis to be inconsistent with the actual natural frequency, which was also a content that needed to be explored and analyzed in the future.
- The Conghua Bridge measured by the field experiment in this paper was a suspender bridge, not a real cable-stayed bridge. Although the measurement methods of

Table 4. Summary of the results of different measurement methods of cable force testing.

Suspender number	Design cable force value(kN)	Measurement method (Relative error (%))		
		Vibration frequency method test value (kN)	Fixed camera test value (kN)	UAV test value (kN)
N5	1411	1335 (-5.39%)	1322 (-6.31%)	1269 (-10.06%)
N6	1376	1178 (-14.39%)	1184 (-13.95%)	1164 (-15.41%)
N7	1318	990 (-24.89%)	980 (-25.64%)	983 (-25.42%)
N8	1376	1141 (-17.08%)	1135 (-17.51%)	1133 (-17.66%)

the suspender and cable were the similar, considering the differences in physical parameters and mechanical properties of the two, it was necessary to apply the method proposed in this paper to carry out actual measurements on a cable-stayed bridge in the future to further verify the feasibility of this method.

- On the accurate calculation of cable force. The purpose of this study was to propose a method for the cable force measurement based on the natural frequency of the cable vibration. In order to accurately measure the cable force, factors such as the boundary conditions at both ends of the cable, the bending stiffness of the cable, the sag, the angle of inclination and the length must be taken into account. Section 2.3 used a simplified formula for calculating cable force, but actually calculating cable force in this way was inaccurate because it simplified the boundary conditions, ignored the effect of the bending stiffness, and inclination angle of the cable. In the future, more complex empirical formulas considering these factors could be developed to improve the accuracy of the cable force calculation.
- It could be considered in the future to assess the influence of wind on cable force measurement. External wind was one of the most common environmental factors during UAV flight. The strength and direction of the wind could affect the flight stability and vibration of the UAV. Therefore, it was necessary to consider the vibrations caused by external wind in the experiments.
- The impact when vehicles passed by. When vehicles, especially large ones, passed by, their movement introduced additional forces and vibrations that could interfere with the accurate measurement of tension. In the future, relevant experiments could be designed to consider the influence of passing vehicles, especially large vehicles, on tension measurement.

4.2 Conclusions

In this study, the KLT optical flow technique was employed to track the predetermined target points on the bridge cables and extract the displacement-time-history curve. Subsequently, the EMD method was used to decompose the displacement-time-history curve into several IMF components and residue, and the true vibration signals of the cable were determined by modal analysis of these IMF components. Then, the OMA was

used to process the vibration signals of the target point to obtain the PSD curve of the cable. Finally, the peak extraction method was employed to extract the natural frequencies of the cable from the PSD curve, and the cable force value was obtained based on the vibration equation theory. The specific conclusions were as follows:

- Traditional contact-based measurement of cable force on bridges required accelerometers to be manually installed on the cables, which was inefficient and had certain safety risks. UAVs had the advantages of easy operation and the ability to hover in any position, which had significant advantages in measuring cable vibration.
- The EMD method was used to achieve fast solution of the dynamic displacement response of bridge cables, overcoming the problem of complexity and the need for fixed reference points in traditional displacement correction methods. By comparing with the FT-IFT method, the superiority of the EMD method in solving the cable modal parameters was verified.
- The effectiveness of the method was verified by using the cable model and experimental data from the Conghua Bridge. The results showed that the natural frequencies of the cable obtained by the UAV technology had a relative error of less than 5% compared with that obtained by the fixed camera and accelerometers, which successfully verified the correctness of the cable force measurement method proposed in this article.

In summary, the use of UAVs combined with the EMD method was more promising than accelerometers and fixed cameras for cable force measurement. This method could be applied to some situations that were difficult to use fixed cameras and accelerometers, such as cross-sea and cross-mountain bridges.

Funding

None.

Conflict of Interest

The authors declare that they have no known competing financial interests or personal relationships that could have appeared to influence the work reported in this paper.

Data availability statement

Some or all data, models, or code generated or used during the study are available from the corresponding author by request.

Author contribution statement

Wenjun Luo (First Author): Conceptualization, Data Curation, Formal Analysis, Methodology, Software, Investigation, Writing - Original Draft; Shufan Cai: Conceptualization, Formal Analysis, Methodology, Software, Resources, Visualization; Limei Zeng: Data Curation, Formal Analysis; Gongfa Chen (Corresponding Author): Supervision, Writing - Review & Editing; David Bassir: Supervision, Writing - Review & Editing.

References

- L. Zhang, G. Qiu, Z. Chen, Structural health monitoring methods of cables in cable-stayed bridge: a review, *Measurement* **168**, 108343 (2021)
- A. Cunha, E. Caetano, R. Delgado, Dynamic tests on large cable-stayed bridge, *J. Bridge Eng.* **6**, 54–62 (2001)
- W.-X. Ren, X.-L. Peng, Y.-Q. Lin, Experimental and analytical studies on dynamic characteristics of a large span cable-stayed bridge, *Eng. Struct.* **27**, 535–548 (2005)
- C. Yang, K. Liang, X. Zhang, X. Geng, Sensor placement algorithm for structural health monitoring with redundancy elimination model based on sub-clustering strategy, *Mech. Syst. Signal Process.* **124**, 369–387 (2019)
- C. Yang, Y. Xia, A novel two-step strategy of non-probabilistic multi-objective optimization for load-dependent sensor placement with interval uncertainties, *Mech. Syst. Signal Process.* **176**, 109173 (2022)
- L. Li, T. Ohkubo, S. Matsumoto, Vibration measurement of a steel building with viscoelastic dampers using acceleration sensors, *Measurement* **171**, 108807 (2021)
- P. Psimoulis, S. Pytharouli, D. Karambalis, S. Stiros, Potential of global positioning system (GPS) to measure frequencies of oscillations of engineering structures, *J. Sound Vib.* **318**, 606–623 (2008)
- D.M. Siringoringo, Y. Fujino, Noncontact operational modal analysis of structural members by laser Doppler vibrometer, *Comput. Aided Civil Infrastruct. Eng.* **24**, 249–265 (2009)
- D. Lydon, M. Lydon, S. Taylor, J.M. Del Rincon, D. Hester, J. Brownjohn, Development and field testing of a vision-based displacement system using a low cost wireless action camera, *Mech. Syst. Signal Process.* **121**, 343–358 (2019)
- H. Yoon, H. Elanwar, H. Choi, M. Golparvar-Fard, B.F. Spencer Jr, Target-free approach for vision-based structural system identification using consumer-grade cameras, *Struct. Control Health Monitor.* **23**, 1405–1416 (2016)
- S. Yoneyama, Basic principle of digital image correlation for in-plane displacement and strain measurement, *Adv. Compos. Mater.* **25**, 105–123 (2016)
- W. Du, D. Lei, P. Bai, F. Zhu, Z. Huang, Dynamic measurement of stay-cable force using digital image techniques, *Measurement* **151**, 107211 (2020)
- F. Xiao, R. Zhao, P. Sun, Three-dimensional displacement measurement based on the combination of digital image correlation and optical flow, *Appl. Opt.* **55**, 8207–8212 (2016)
- Y.J. Cha, J.G. Chen, O. Büyüköztürk, Output-only computer vision based damage detection using phase-based optical flow and unscented Kalman filters, *Eng. Struct.* **132**, 300–313 (2017)
- G. Chen, Q. Liang, W. Zhong, X. Gao, F. Cui, Homography-based measurement of bridge vibration using UAV and DIC method, *Measurement* **170**, 108683 (2021)
- G. Deng, Z. Zhou, S. Shao, X. Chu, C. Jian, A novel dense full-field displacement monitoring method based on image sequences and optical flow algorithm, *Appl. Sci.* **10**, 2018 (2020)
- J. Zhu, Z. Lu, C. Zhang, A marker-free method for structural dynamic displacement measurement based on optical flow, *Struct. Infrastruct. Eng.* **18**, 84–96 (2022)
- S. Jianbo, Tomasi, Good features to track, 1994 Proceedings of IEEE Conference on Computer Vision and Pattern Recognition (1994), pp. 593–600
- Z. Yan, Z. Jin, S. Teng, G. Chen, D. Bassir, Measurement of bridge vibration by UAVs combined with CNN and KLT optical-flow method, *Appl. Sci.* **12**, 5181 (2022)
- C.-Z. Dong, O. Celik, F.N. Catbas, E.J. O'Brien, S. Taylor, Structural displacement monitoring using deep learning-based full field optical flow methods, *Struct. Infrastruct. Eng.* **16**, 51–71 (2020)
- Z. Yan, S. Teng, W. Luo, D. Bassir, G. Chen, Bridge modal parameter identification from UAV measurement based on empirical mode decomposition and Fourier transform, *Appl. Sci.* **12**, 8689 (2022)
- I.-H. Kim, H.-J. Jung, S. Yoon, J.W. Park, Dynamic response measurement and cable tension estimation using an unmanned aerial vehicle, *Remote Sens.* **15**, 4000 (2023)
- J.S. Myeong, B. Yu et al., Development of wall-climbing unmanned aerial vehicle system for micro-inspection of bridges, in *International Conference on Robotics and Automation (ICRA)* (2019), pp. 20–24
- R.M. Bhatwdekar, S. Choudhury, E.T. Modmad, UAV applications on projects monitoring in mining and civil engineering, *J. Mines Metals Fuels* **66**, 867–878 (2018)
- P. Biswakarma, A. Kainthola, R.M. Bhatwdekar, V. Joshi, E.T. Mohamad, Unmanned aerial vehicles technology for slope hazard assessment, monitoring, and post failure management, *Landslides: Detection, Prediction and Monitoring: Technological Developments* (2023), 365–381
- M.E.T. Bhatwdekar, R.M. Singh, Selection of Lidar technology for limestone quarry in Thailand, *J. Mines Metals Fuels* **65** (2017)
- C. Yang, W. Lu, Y. Xia, Reliability-constrained optimal attitude-vibration control for rigid-flexible coupling satellite using interval dimension-wise analysis, *Reliab. Eng. Syst. Saf.* **237**, 109382 (2023)
- C. Yang, W. Lu, Y. Xia, Uncertain optimal attitude control for space power satellite based on interval Riccati equation with non-probabilistic time-dependent reliability, *Aerospace Sci. Technol.* **139**, 108406 (2023)
- Z. Wu, G. Chen, Q. Ding, B. Yuan, X. Yang, Three-dimensional reconstruction-based vibration measurement of bridge model using UAVs, *Appl. Sci.* **11**, 5111 (2021)

30. V. Hoskere, J.-W. Park, H. Yoon, F. Spencer Billie, Vision-based modal survey of civil infrastructure using unmanned aerial vehicles, *J. Struct. Eng.* **145**, 04019062 (2019)
31. H.-C. Lin, Y.-C. Ye, Reviews of bearing vibration measurement using fast Fourier transform and enhanced fast Fourier transform algorithms, *Adv. Mech. Eng.* **11**, 1687814018816751 (2019)
32. J.A. Lazaro, R. Wessel, J. Koppenborg, G. Dudziak, I.J. Blewett, Inverse Fourier transform method for characterizing arrayed-waveguide gratings, *IEEE Photonics Technol. Lett.* **15**, 93–95 (2003)
33. Y. Tian, C. Zhang, S. Jiang, J. Zhang, W. Duan, Noncontact cable force estimation with unmanned aerial vehicle and computer vision, *Comput. Aided Civil Infrastruct. Eng.* **36**, 73–88 (2021)
34. N.E. Huang, Z. Shen, S.R. Long, M.C. Wu, H.H. Shih, Q. Zheng, N.-C. Yen, C.C. Tung, H.H. Liu, The empirical mode decomposition and the Hilbert spectrum for nonlinear and non-stationary time series analysis, *Proc. Royal Soc. London Ser. A* **454**, 903–995 (1971)
35. J. Chen, Y.L. Xu, R.C. Zhang, Modal parameter identification of Tsing Ma suspension bridge under Typhoon Victor: EMD-HT method, *J. Wind Eng. Ind. Aerodyn.* **92**, 805–827 (2004)
36. W.-J. Yan, W.-X. Ren, An enhanced power spectral density transmissibility (EPSDT) approach for operational modal analysis: theoretical and experimental investigation, *Eng. Struct.* **102**, 108–119 (2015)
37. W.-J. Yan, W.-X. Ren, Operational modal parameter identification from power spectrum density transmissibility, *Comput. Aided Civil Infrastruct. Eng.* **27**, 202–217 (2012)
38. P. Mohanty, D.J. Rixen, Identifying mode shapes and modal frequencies by operational modal analysis in the presence of harmonic excitation, *Exp. Mech.* **45**, 213–220 (2005)
39. Q. Sun, W. Yan, W. Ren, Operational modal analysis for bridge engineering based on power spectrum density transmissibility, *China J. Highway Transport* 83–90 (2020)
40. B.H. Kim, T. Park, Estimation of cable tension force using the frequency-based system identification method, *J. Sound Vibrat.* **304**, 660–676 (2007)
41. H. Yoon, J. Shin, B.F. Spencer Jr, Structural displacement measurement using an unmanned aerial system, *Comput. Aided Civil Infrastruct. Eng.* **33**, 183–192 (2018)
42. C. Devriendt, P. Guillaume, The use of transmissibility measurements in output-only modal analysis, *Mech. Syst. Signal Process.* **21**, 2689–2696 (2007)
43. G. Chen, Z. Wu, C. Gong, J. Zhang, X. Sun, DIC-based operational modal analysis of bridges, *Adv. Civil Eng.* 2021, 6694790 (2021)
44. Y. Wang, K. Li, Y. Chen, S. Xu, W. Shou, Research on non-contact and non-fixed cable force measurement based on smartphone, *Appl. Sci.* **11** (2021)
45. W.S.J.A.S. Cleveland, LOWESS: a program for smoothing scatterplots by robust locally weighted regression, *J. Am. Stat. Assoc.* **35**, 54–54 (1981)

Cite this article as: Wenjun Luo, Shufan Cai, Limei Zeng, Gongfa Chen, David Bassir, Cable force estimation method based on UAVs and EMD, *Int. J. Simul. Multidisci. Des. Optim.* **15**, 14 (2024)